

# Precision Measurements of the Nucleon Strange Form Factors at $Q^2 \sim 0.1 \text{ GeV}^2$

A. Acha,<sup>1</sup> K. A. Aniol,<sup>2</sup> D. S. Armstrong,<sup>3</sup> J. Arrington,<sup>4</sup> T. Averett,<sup>3</sup> S. L. Bailey,<sup>3</sup> J. Barber,<sup>5</sup> A. Beck,<sup>6</sup> H. Benaoum,<sup>7</sup> J. Benesch,<sup>8</sup> P. Y. Bertin,<sup>9</sup> P. Bosted,<sup>8</sup> F. Butaru,<sup>10</sup> E. Burtin,<sup>11</sup> G. D. Cates,<sup>12</sup> Y.-C. Chao,<sup>8</sup> J.-P. Chen,<sup>8</sup> E. Chudakov,<sup>8</sup> E. Cisbani,<sup>13</sup> B. Craver,<sup>12</sup> F. Cusanno,<sup>13</sup> R. De Leo,<sup>14</sup> P. Decowski,<sup>15</sup> A. Deur,<sup>8</sup> R. J. Feuerbach,<sup>8</sup> J. M. Finn,<sup>3</sup> S. Frullani,<sup>13</sup> S. A. Fuchs,<sup>3</sup> K. Fuoti,<sup>5</sup> R. Gilman,<sup>16,8</sup> L. E. Glesener,<sup>3</sup> K. Grimm,<sup>3</sup> J. M. Grames,<sup>8</sup> J. O. Hansen,<sup>8</sup> J. Hansknecht,<sup>8</sup> D. W. Higinbotham,<sup>8</sup> R. Holmes,<sup>7</sup> T. Holmstrom,<sup>3</sup> H. Ibrahim,<sup>17</sup> C. W. de Jager,<sup>8</sup> X. Jiang,<sup>16</sup> J. Katich,<sup>3</sup> L. J. Kaufman,<sup>5</sup> A. Kelleher,<sup>3</sup> P. M. King,<sup>18</sup> A. Kolarkar,<sup>19</sup> S. Kowalski,<sup>6</sup> E. Kuchina,<sup>16</sup> K. S. Kumar,<sup>5</sup> L. Lagamba,<sup>14</sup> P. LaViolette,<sup>5</sup> J. LeRose,<sup>8</sup> R. A. Lindgren,<sup>12</sup> D. Lhuillier,<sup>11</sup> N. Liyanage,<sup>12</sup> D. J. Margaziotis,<sup>2</sup> P. Markowitz,<sup>1</sup> D. G. Meekins,<sup>8</sup> Z.-E. Meziani,<sup>10</sup> R. Michaels,<sup>8</sup> B. Moffit,<sup>3</sup> S. Nanda,<sup>8</sup> V. Nelyubin,<sup>12,20</sup> K. Otis,<sup>5</sup> K. D. Paschke,<sup>5</sup> S. K. Phillips,<sup>3</sup> M. Poelker,<sup>8</sup> R. Pomatsalyuk,<sup>21</sup> M. Potokar,<sup>22</sup> Y. Prok,<sup>12</sup> A. Puckett,<sup>6</sup> Y. Qian,<sup>23</sup> Y. Qiang,<sup>6</sup> B. Reitz,<sup>8</sup> J. Roche,<sup>8</sup> A. Saha,<sup>8</sup> B. Sawatzky,<sup>10</sup> J. Singh,<sup>12</sup> K. Slifer,<sup>10</sup> S. Sirca,<sup>6</sup> R. Snyder,<sup>12</sup> P. Solvignon,<sup>10</sup> P. A. Souder,<sup>7</sup> M. L. Stutzman,<sup>8</sup> R. Subedi,<sup>24</sup> R. Suleiman,<sup>6</sup> V. Sulkosky,<sup>3</sup> W. A. Tobias,<sup>12</sup> P. E. Ulmer,<sup>17</sup> G. M. Urciuoli,<sup>13</sup> K. Wang,<sup>12</sup> A. Whitbeck,<sup>8</sup> R. Wilson,<sup>25</sup> B. Wojtsekhowski,<sup>8</sup> H. Yao,<sup>10</sup> Y. Ye,<sup>26</sup> X. Zhan,<sup>6</sup> X. Zheng,<sup>6,4</sup> S. Zhou,<sup>27</sup> and V. Ziskin<sup>6</sup>

(The HAPPEX Collaboration)

<sup>1</sup> Florida International University, Miami, Florida 33199, USA

<sup>2</sup> California State University, Los Angeles, Los Angeles, California 90032, USA

<sup>3</sup> College of William and Mary, Williamsburg, Virginia 23187, USA

<sup>4</sup> Argonne National Laboratory, Argonne, Illinois 60439, USA

<sup>5</sup> University of Massachusetts Amherst, Amherst, Massachusetts 01003, USA

<sup>6</sup> Massachusetts Institute of Technology, Cambridge, Massachusetts 02139, USA

<sup>7</sup> Syracuse University, Syracuse, New York 13244, USA

<sup>8</sup> Thomas Jefferson National Accelerator Facility, Newport News, Virginia 23606, USA

<sup>9</sup> Université Blaise Pascal/CNRS-IN2P3, F-63177 Aubièrre, France

<sup>10</sup> Temple University, Philadelphia, Pennsylvania 19122, USA

<sup>11</sup> CEA Saclay, DAPNIA/SPhN, F-91191 Gif-sur-Yvette, France

<sup>12</sup> University of Virginia, Charlottesville, Virginia 22904, USA

<sup>13</sup> Istituto Nazionale di Fisica Nucleare, Sezione Sanità, 00161 Roma, Italy

<sup>14</sup> Istituto Nazionale di Fisica Nucleare, Sezione di Bari and University of Bari, I-70126 Bari, Italy

<sup>15</sup> Smith College, Northampton, Massachusetts 01063, USA

<sup>16</sup> Rutgers, The State University of New Jersey, Piscataway, New Jersey 08855, USA

<sup>17</sup> Old Dominion University, Norfolk, Virginia 23529, USA

<sup>18</sup> University of Illinois, Urbana, Illinois 61801, USA

<sup>19</sup> University of Kentucky, Lexington, Kentucky 40506, USA

<sup>20</sup> St. Petersburg Nuclear Physics Institute of Russian Academy of Science, Gatchina, 188350, Russia

<sup>21</sup> Kharkov Institute of Physics and Technology, Kharkov 310108, Ukraine

<sup>22</sup> Jozef Stefan Institute, 1000 Ljubljana, Slovenia

<sup>23</sup> Duke University, Durham, North Carolina 27706, USA

<sup>24</sup> Kent State University, Kent, Ohio 44242, USA

<sup>25</sup> Harvard University, Cambridge, Massachusetts 02138, USA

<sup>26</sup> University of Science and Technology of China, Hefei, Anhui 230026, China

<sup>27</sup> China Institute of Atomic Energy, Beijing 102413, China

(Dated: September 4, 2006)

We report new measurements of the parity-violating asymmetry  $A_{PV}$  in elastic scattering of 3 GeV electrons off hydrogen and  $^4\text{He}$  targets with  $\langle\theta_{lab}\rangle \approx 6.0^\circ$ . The  $^4\text{He}$  result is  $A_{PV} = (+6.40 \pm 0.23 \text{ (stat)} \pm 0.12 \text{ (syst)}) \times 10^{-6}$ . The hydrogen result is  $A_{PV} = (-1.58 \pm 0.12 \text{ (stat)} \pm 0.04 \text{ (syst)}) \times 10^{-6}$ . These results significantly improve constraints on the electric and magnetic strange form factors  $G_E^s$  and  $G_M^s$ . We extract  $G_E^s = 0.002 \pm 0.014 \pm 0.007$  at  $\langle Q^2 \rangle = 0.077 \text{ GeV}^2$ , and  $G_E^s + 0.09 G_M^s = 0.007 \pm 0.011 \pm 0.006$  at  $\langle Q^2 \rangle = 0.109 \text{ GeV}^2$ , providing new limits on the role of strange quarks in the nucleon charge and magnetization distributions.

PACS numbers: 25.30.Bf, 13.60.Fz, 11.30.Er, 13.40.Gp, 14.20.Dh

Over the past several decades, high-energy lepton-nucleon scattering has revealed the rich structure of the nucleon over a wide range of length scales. In recent years, increasingly sensitive measurements of elas-

tic electron-nucleon scattering, mediated by photon exchange and  $Z^0$  exchange, have enabled the measurement of the electromagnetic and neutral weak form factors. These functions of the 4-momentum transfer  $Q^2$  charac-

terize nucleon charge and magnetization distributions.

In particular, the neutral weak form factor measurements provide a way to probe dynamics of the “sea” of virtual light (up, down and strange) quark-antiquark pairs that surrounds each valence quark in the nucleon. Since the  $Z^0$  boson couples to various quarks with different relative strengths compared to the photon, a combined analysis of proton and neutron electromagnetic form factor and proton neutral weak form factor measurements, along with the assumption of charge symmetry, allows the determination of the strange electric and magnetic form factors  $G_E^s$  and  $G_M^s$  [1, 2].

The established experimental technique to measure the electron-nucleon weak neutral current amplitude is parity-violating electron scattering [3, 4]. Longitudinally-polarized electron-scattering off unpolarized targets can access a parity-violating asymmetry  $A_{PV} \equiv (\sigma_R - \sigma_L)/(\sigma_R + \sigma_L)$ , where  $\sigma_{R(L)}$  is the cross section for incident right(left)-handed electrons. Arising from the interference of the weak and electromagnetic amplitudes,  $A_{PV}$  increases with  $Q^2$  [5].

Four experimental programs have been designed to access the  $Q^2$  range of 0.1 to 1 GeV<sup>2</sup>, where the  $A_{PV}$  expectations range from one to tens of parts per million (ppm). The published measurements [6–12] are mutually consistent. An intriguing pattern in the low- $Q^2$  behavior seen in [9, 10] has marginal statistical significance.

In this paper, we significantly improve our two previous measurements [11, 12] of  $A_{PV}$  in elastic electron scattering from  $^1\text{H}$  and  $^4\text{He}$  nuclei. Since  $A_{PV}$  for  $^1\text{H}$  is sensitive to a linear combination of  $G_E^s$  and  $G_M^s$  while that for  $^4\text{He}$  is sensitive only to  $G_E^s$ , a simultaneous analysis of both measurements results in the most precise determination to date of  $G_E^s$  and  $G_M^s$  at  $Q^2 \sim 0.1$  GeV<sup>2</sup>.

The measurements were carried out in Hall A at the Thomas Jefferson National Accelerator Facility (JLab). As described in detail in two previous publications [11, 12], a 35 to 55  $\mu\text{A}$  continuous-wave beam of  $\sim 3$  GeV longitudinally polarized electrons was incident on 20 cm long cryogenic targets. Elastically scattered electrons were focused into background-free regions by a symmetric pair of high-resolution spectrometer systems. The scattered flux was intercepted by identical detector segments in each arm (two for  $^1\text{H}$ , one for  $^4\text{He}$ ), resulting in Cherenkov light collected by photomultiplier tubes (PMTs).

The helicity of the electron beam, generated by photoemission off a GaAs wafer, is determined by the handedness of the incident laser light’s circular polarization. This was selected pseudorandomly at 15 Hz and toggled to the opposing helicity after 33.3 ms, with each of these equal periods of constant helicity referred to as a “window.” PMT and beam monitor responses for two consecutive windows of opposite helicity were integrated, digitized, and grouped as a “pair” for asymmetry analysis.

The beam monitors, target, detector components, electronics and accelerator tune were optimized such that the

	Helium	Hydrogen
$A_{\text{Intensity}}$	-0.377 ppm	0.406 ppm
$A_{\text{Energy}}$	3 ppb	0.2 ppb
$\Delta x$	-0.2 nm	0.5 nm
$\Delta x'$	4.4 nrad	-0.2 nrad
$\Delta y$	-26 nm	1.7 nm
$\Delta y'$	-4.4 nrad	0.2 nrad

TABLE I: Average beam asymmetries under polarization reversal in intensity and energy and differences in horizontal and vertical position ( $\Delta x$ ,  $\Delta y$ ) and angle ( $\Delta x'$ ,  $\Delta y'$ ).

fluctuation in the PMT response over a pair was dominated by counting statistics of the scattered flux for rates up to 100 MHz. This facilitated  $A_{PV}$  measurements with statistical uncertainty as small as 100 parts per billion (ppb) in a reasonable length of time. To keep spurious beam-induced asymmetries under control at this level, the laser optics leading to the photocathode were carefully designed and monitored. Indeed, averaged over the entire period of data collection with the hydrogen target, the achieved level of control surpassed all previous benchmarks, as summarized in Table I.

The data collection took place over 55 days ( $^4\text{He}$ ) and 36 days ( $^1\text{H}$ ). A half-wave ( $\lambda/2$ ) plate was periodically inserted into the laser optical path which passively reversed the sign of the electron beam polarization. With roughly equal statistics in each state, many systematic effects were suppressed. There were 121 ( $^4\text{He}$ ) and 41 ( $^1\text{H}$ ) such reversals. The data set between two successive  $\lambda/2$  reversals is referred to as a “slug.”

Loose requirements were imposed on beam quality to remove periods of instability, leaving about 95% of the data sample for further analysis. No helicity-dependent cuts were applied. The final data sample consisted of  $35.0 \times 10^6$  ( $^4\text{He}$ ) and  $26.4 \times 10^6$  ( $^1\text{H}$ ) pairs. The right-left helicity asymmetry in the integrated detector response, normalized to the beam intensity, was computed for each pair to form the raw asymmetry  $A_{\text{raw}}$ . The dependence of  $A_{\text{raw}}$  on fluctuations in the five correlated beam parameter differences  $\Delta x_i$  is quantified as  $A_{\text{beam}} = \sum c_i \Delta x_i$ , where the coefficients  $c_i$  quantify the  $A_{\text{raw}}$  beam parameter sensitivity. The electroweak physics of the signal and backgrounds is contained in  $A_{\text{corr}} = A_{\text{raw}} - A_{\text{beam}}$ .

The  $A_{\text{corr}}$  window-pair distributions for the two complete data samples were perfectly Gaussian over more than 4 orders of magnitude with RMS widths of 1130 ppm ( $^4\text{He}$ ) and 540 ppm ( $^1\text{H}$ ); the dominant source of noise in the PMT response was counting statistics. To further test that the data behaved statistically and the errors were being accurately calculated,  $A_{\text{corr}}$  averages and statistical errors for typical one hour runs, consisting of about 50k pairs each, were studied. Each set of roughly 400 average  $A_{\text{corr}}$  values, normalized by the corresponding statistical errors, populated a Gaussian distribution of unit variance as expected.

	$\lambda/2$ OUT		$\lambda/2$ IN		BOTH	
$^4\text{He}$	(DOF = 59)		(DOF = 60)		(DOF = 120)	
	Asym	$r\chi^2$	Asym	$r\chi^2$	Asym	$r\chi^2$
$A_{\text{raw}}$	$4.80 \pm 0.27$	0.75	$-5.41 \pm 0.27$	1.12	$5.10 \pm 0.19$	0.95
$A_{\text{corr}}$	$5.12 \pm 0.27$	0.78	$-5.38 \pm 0.27$	1.07	$5.25 \pm 0.19$	0.92
$^1\text{H}$	(DOF = 20)		(DOF = 19)		(DOF = 40)	
	Asym	$r\chi^2$	Asym	$r\chi^2$	Asym	$r\chi^2$
$A_{\text{raw}}$	$-1.40 \pm 0.15$	0.73	$1.42 \pm 0.15$	1.04	$-1.41 \pm 0.11$	0.86
$A_{\text{corr}}$	$-1.41 \pm 0.15$	0.81	$1.43 \pm 0.15$	1.02	$-1.42 \pm 0.11$	0.89

TABLE II: Raw and corrected asymmetries (in ppm) and reduced “slug”  $\chi^2$  ( $r\chi^2$ ), broken up by  $\lambda/2$  reversals. The differences between  $A_{\text{raw}}$  and  $A_{\text{corr}}$  result from corrections for energy, position, and angle differences which are summarized in Table I.

Systematic effects in  $A_{\text{beam}}$  estimations were studied. When averaged over all detector segments, the coefficients  $c_i$  were much smaller than those for individual detector segments due to the symmetric geometry of the apparatus. Limits on systematic uncertainties in the  $c_i$ 's in the range of 10 to 30% were set by inspecting residual correlations of  $A_{\text{corr}}$ 's of individual detector segments with helicity-correlated beam asymmetries.

Another important validation was to use two independent methods to calculate  $c_i$ . The first relied on linear regression of the observed response of the detector PMTs to intrinsic beam fluctuations. The other used calibration data in which the beam was modulated, by amounts large compared to intrinsic beam fluctuations, using steering magnets and an accelerating cavity. Differences in the two  $A_{\text{beam}}$  calculations were always much smaller than corresponding  $A_{\text{corr}}$  statistical errors.

Final  $A_{\text{corr}}$  results were calculated using the beam modulation technique and are summarized in Table II. Due to the excellent control of beam parameter differences  $\Delta x_i$  summarized in Table I,  $A_{\text{corr}} - A_{\text{raw}}$  values are of the order of, or much smaller than, the corresponding statistical errors. Under  $\lambda/2$  reversal, the absolute values of  $A_{\text{corr}}$  are consistent within statistical errors. The reduced  $\chi^2$  for  $A_{\text{corr}}$  “slug” averages is close to one in every case, indicating that any residual beam-related systematic effects were small and randomized over the time period of  $\lambda/2$  reversals (typically 5 to 10 hours). The final  $A_{\text{corr}}$  results are  $A_{\text{corr}}^{\text{He}} = +5.25 \pm 0.19(\text{stat}) \pm 0.05(\text{syst})$  ppm and  $A_{\text{corr}}^{\text{H}} = -1.42 \pm 0.11(\text{stat}) \pm 0.02(\text{syst})$  ppm.

The physics asymmetry  $A_{\text{phys}}$  is formed from  $A_{\text{corr}}$ ,

$$A_{\text{phys}} = \frac{K}{P_b} \frac{A_{\text{corr}} - P_b \sum_i A_i f_i}{1 - \sum_i f_i}, \quad (1)$$

with corrections for the beam polarization  $P_b$ , background fractions  $f_i$  with asymmetries  $A_i$  and finite kinematic acceptance  $K$ . These corrections are described below and summarized in Table III. The first line lists the cumulative  $A_{\text{beam}}$  corrections discussed above, scaled by  $K/P_b$ .

A powerful feature of the apparatus is the spectrom-

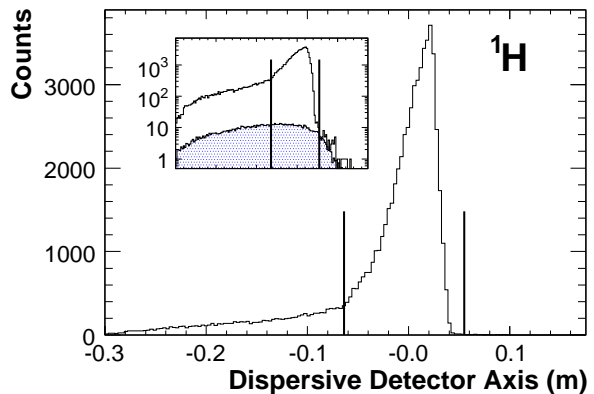
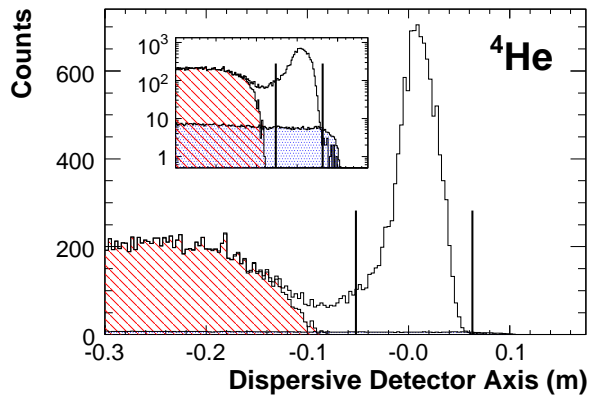


FIG. 1: Single-particle spectra obtained in dedicated low-current runs. The insets show the same spectra on a logarithmic scale. The vertical lines delineate the extent of the detectors. Inelastic scattering from  $^4\text{He}$  is entirely contained in the hatched area. The shaded regions, visible only in the log plots, show the contribution from target windows.

Correction (ppb)	Helium	Hydrogen
Beam Asyms.	$183 \pm 59$	$-10 \pm 17$
Target window bkg.	$113 \pm 32$	$7 \pm 19$
Helium QE bkg.	$12 \pm 20$	-
Rescatter bkg.	$20 \pm 15$	$2 \pm 4$
Nonlinearity	$0 \pm 58$	$0 \pm 15$
Scale Factor	Helium	Hydrogen
Acceptance factor $K$	$1.000 \pm 0.001$	$0.979 \pm 0.002$
$Q^2$ Scale	$1.000 \pm 0.009$	$1.000 \pm 0.017$
Polarization $P_b$	$0.844 \pm 0.008$	$0.871 \pm 0.009$

TABLE III: Corrections to  $A_{\text{corr}}$  and systematic errors.

eters’ ability to focus the elastically scattered electrons into a compact region. Indeed, much less than 1% of the flux intercepted by the detectors originated from inelastic scattering in the target cryogen. Figure 1 shows charged particle spectra obtained with dedicated low-intensity runs and measured by drift chambers in front of the detectors. The dominant background was quasi-elastic scattering from target windows, separately measured using an equivalent aluminum target and computed

to be  $1.8 \pm 0.2\%$  ( $^4\text{He}$ ) and  $0.76 \pm 0.25\%$  ( $^1\text{H}$ ).

An electron must give up more than 19 MeV to break up the  $^4\text{He}$  nucleus and undergo quasi-elastic scattering off nucleons. Figure 1 shows that the quasi-elastic threshold lies beyond the edge of the detector. A limit of  $0.15 \pm 0.15\%$  on this background was placed by detailed studies of the low-intensity data. For  $^1\text{H}$ , the  $\pi^0$  threshold is beyond the extent of the plot; direct background from inelastic scattering is thus negligible.

Background from rescattering in the spectrometer apertures was studied by varying the spectrometer momentum in dedicated runs to measure inelastic spectra and to obtain the detector response as a function of scattered electron energy under running conditions. From these two distributions, the rescattering background was estimated to be  $0.25 \pm 0.15\%$  ( $^4\text{He}$ ) and  $0.10 \pm 0.05\%$  ( $^1\text{H}$ ).

For each source of background, a theoretical estimate for  $A_{\text{PV}}$  was used, with relative uncertainties taken to be 100% or more to account for kinematic variations and resonance contributions. The resulting corrections and the associated errors are shown in Table III. Upper limits on rescattering contributions from exposed iron in the spectrometer led to an additional uncertainty of 5 ppb.

Nonlinearity in the PMT response was limited to 1% in bench-tests that mimicked running conditions. The relative nonlinearity between the PMT response and those of the beam intensity monitors was  $< 2\%$ . A nuclear recoil technique using a water-cell target [11] was used to determine the scattering angle  $\theta_{\text{lab}}$ , thus keeping the scale error on  $\langle Q^2 \rangle$  due to  $\theta_{\text{lab}}$  to be  $< 0.2\%$ . The acceptance correction  $K$  accounted for the non-linear dependence of the asymmetry with  $Q^2$ .

The beam polarization,  $P_b$ , was continuously monitored by a Compton polarimeter; results, averaged over the duration of each run, are listed in Tab. III. Redundant cross-calibration of the recoil Compton electron spectrum restricted the relative systematic error to  $\approx 1\%$ . The results were consistent, within systematic uncertainties, with those obtained from recoil Compton photon asymmetries, and with dedicated measurements using Møller scattering in the experimental hall and Mott scattering at low energy. Throughout the asymmetry and background analysis, blinding offsets were maintained on both results. These offsets, which were significantly larger than the respective statistical errors, were removed only after all analysis tasks were completed. After all corrections:

$$\begin{aligned} A_{\text{phys}}^{\text{He}} &= +6.40 \pm 0.23 \text{ (stat)} \pm 0.12 \text{ (syst)} \text{ ppm}, \\ A_{\text{phys}}^{\text{H}} &= -1.58 \pm 0.12 \text{ (stat)} \pm 0.04 \text{ (syst)} \text{ ppm}. \end{aligned}$$

The theoretical predictions  $A_{\text{NS}}^{\text{He}}$  and  $A_{\text{NS}}^{\text{H}}$  with  $G^s = 0$  were estimated using the formalism in [4] and described in our previous publications [11, 12]. The electroweak radiative corrections, calculated using the  $\overline{\text{MS}}$  renormalization scheme, introduced negligible uncertainties.

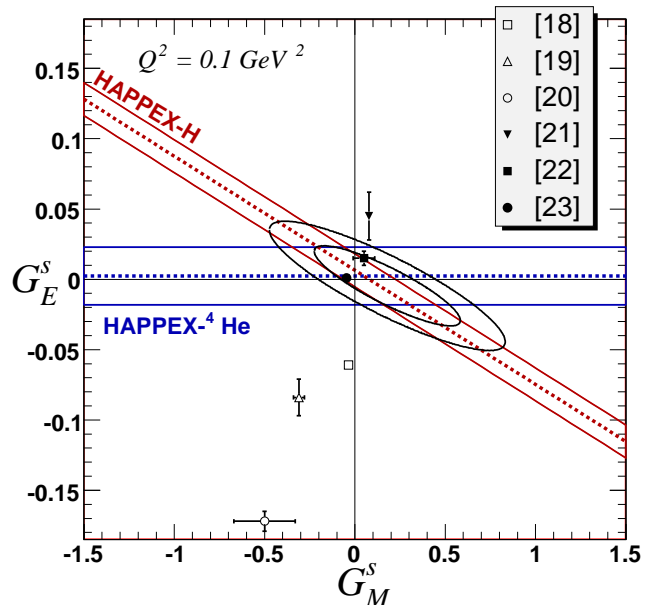


FIG. 2: 68 and 95% C.L. constraints in the  $G_E^s - G_M^s$  plane from data from this apparatus ([11, 12] and this Letter). Various theoretical predictions are plotted with published uncertainty estimates, when available. The 1- $\sigma$  bands (a quadrature sum of statistical and systematic errors) and central values (dashed lines) from the new results alone are also shown.

Assuming a pure isoscalar  $0^+ \rightarrow 0^+$  transition,  $A_{\text{NS}}^{\text{He}}$  is completely independent of nuclear structure and determined purely by electroweak parameters. D-state and isospin admixtures and meson exchange currents are negligible at the level of the experimental fractional accuracy of  $\sim 3\%$  [13]. For our kinematics ( $E_b=2.75$  GeV,  $\langle Q^2 \rangle = 0.077$  GeV $^2$ ) we obtain  $A_{\text{NS}}^{\text{He}} = +6.37$  ppm.

Electromagnetic form factors from a phenomenological fit to the world data at low  $Q^2$  [14] were used to calculate  $A_{\text{NS}}^{\text{H}}$ , with uncertainties governed by data near  $Q^2 \sim 0.1$  GeV $^2$ . The value used for  $G_E^{\gamma n} = 0.037$ , with a 10% relative uncertainty based on new data from the BLAST experiment [15]. For our kinematics ( $E_b=3.18$  GeV,  $\langle Q^2 \rangle = 0.109$  GeV $^2$ ) we obtain  $A_{\text{NS}}^{\text{H}} = -1.66 \pm 0.05$  ppm. This includes a contribution from the axial form factor  $G_A^Z$ , and associated radiative corrections [16], of  $-0.037 \pm 0.018$  ppm.

Comparing our results to the theoretical expectations, we extract  $G_E^s = 0.002 \pm 0.014 \pm 0.007$  at  $Q^2 = 0.077$  GeV $^2$  and  $G_E^s + 0.09G_M^s = 0.007 \pm 0.011 \pm 0.004 \pm 0.005$  (FF) at  $Q^2 = 0.109$  GeV $^2$ , where the uncertainties in the nucleon electromagnetic form factors govern the last error. Figure 2 displays the combined result for these and our previous measurements [11, 12], taken with  $\langle Q^2 \rangle$  between 0.077-0.109 GeV $^2$ . The requisite small extrapolation to a common  $Q^2 = 0.1$  GeV $^2$  was made assuming that  $G_E^s \propto Q^2$  and that  $G_M^s$  is constant. The values  $G_E^s = -0.005 \pm 0.019$  and  $G_M^s = 0.18 \pm 0.27$  (correlation

coefficient  $= -0.87$ ) are obtained. The results are quite insensitive to variations in  $G_A^Z$ , as evidenced by the negligible change induced by an alternate fit similar to that in [17], where  $G_A^Z$  is constrained by other  $A_{PV}$  data.

Figure 2 also displays predictions from selected theoretical models [18–23]. Those that predict little strange quark dynamics in the vector form factors are favored [22, 23]. A global fit to all low- $Q^2$  measurements of  $G_E^s$  and  $G_M^s$ , similar to that performed in [17], finds that other measurements [6, 9, 10] which had suggested non-zero strangeness effects are consistent, within quoted uncertainties, with our results at  $Q^2 = 0.1 \text{ GeV}^2$ . Due to the improved statistical precision and lower  $G_A^Z$  sensitivity of our result, adding these other measurements in a global fit does not alter our conclusions.

In summary, we have reported the most precise constraints on the strange form factors at  $Q^2 \sim 0.1 \text{ GeV}^2$ . The results, consistent within errors with other  $A_{PV}$  measurements, leave little room for observable nucleon strangeness dynamics at low  $Q^2$ . Theoretical uncertainties, especially regarding the assumption of charge symmetry [24], preclude significant improvement to the measurements reported here. While future experiments will pursue the search for non-zero strangeness at higher  $Q^2$ , it now becomes a challenge for various theoretical approaches to reconcile these results and enhance our understanding of nucleon structure.

We wish to thank the entire staff of JLab for their efforts to support this experiment. This work was supported by The Southeastern Universities Research Association, Inc. under U.S. DOE Contract No. DE-AC05-84150, and by the DOE and NSF (United States), the INFN (Italy), and the CEA (France).

---

[1] D.B. Kaplan and A. Manohar, Nucl. Phys. B **310**, 527 (1988).

- [2] R.D. McKeown, Phys. Lett. B **219**, 140 (1989).  
 [3] C.Y. Prescott *et al.*, Phys. Lett. B **77**, 347 (1978).  
 [4] M.J. Musolf *et al.*, Phys. Rep. **239**, 1 (1994).  
 [5] Ya.B. Zel’dovich, Sov. Phys. JETP, **36**, 964 (1959).  
 [6] D.T. Spayde *et al.*, Phys. Lett. B **583**, 79 (2004).  
 [7] K.A. Aniol *et al.*, Phys. Lett. B **509**, 211 (2001);  
 K. A. Aniol *et al.*, Phys. Rev. C **69**, 065501 (2004).  
 [8] F.E. Maas *et al.*, Phys. Rev. Lett. **93**, 022002 (2004).  
 [9] F.E. Maas *et al.*, Phys. Rev. Lett. **94**, 152001 (2005).  
 [10] D.S. Armstrong *et al.*, Phys. Rev. Lett. **95**, 092001 (2005).  
 [11] K.A. Aniol *et al.*, Phys. Rev. Lett. **96**, 022003 (2006).  
 [12] K.A. Aniol *et al.*, Phys. Lett. B **635**, 275 (2006).  
 [13] M.J. Musolf, R. Schiavilla and T.W. Donnelly, Phys. Rev. C **50**, 2173 (1994); S. Ramavataram, E. Hadjimichael and T.W. Donnelly, Phys. Rev. C **50**, 1175 (1994); M.J. Musolf and T.W. Donnelly, Phys. Lett. B **318**, 263 (1993).  
 [14] J. Friedrich and Th. Walcher, Eur. Phys. J. A **17**, 607 (2003).  
 [15] V. Ziskin, PhD. thesis, MIT, 2005.  
 [16] S.-L. Zhu *et al.*, Phys. Rev. D **62**, 033008 (2000).  
 [17] R. Young *et al.*, Phys. Rev. Lett. **97**, 102002 (2006).  
 [18] N.W. Park and H. Weigel, Nucl. Phys. A **451**, 453 (1992).  
 [19] H.W. Hammer, U.G. Meissner, and D. Drechsel, Phys. Lett. B **367**, 323 (1996).  
 [20] H.W. Hammer and M.J. Ramsey-Musolf, Phys. Rev. C **60**, 045204 (1999).  
 [21] A. Silva *et al.*, Phys. Rev. D **65**, 014016 (2001).  
 [22] R. Lewis *et al.*, Phys. Rev. D **67**, 013003 (2003).  
 [23] D.B. Leinweber *et al.*, Phys. Rev. Lett. **94**, 212001 (2005); D.B. Leinweber *et al.*, Phys. Rev. Lett. **97**, 022001 (2006).  
 [24] B. Kubis and R. Lewis, Phys. Rev. C. **74**, 015204 (2006).